(12) INTERNATIONAL APPLICATION PUBLISHED UNDER THE PATENT COOPERATION TREATY (PCT)

(19) World Intellectual Property Organization
International Bureau

(43) International Publication Date
22 December 2005 (22.12.2005)

PCT

(10) International Publication Number
WO 2005/122026 A2

(51) International Patent Classification[7]: G06F 17/50

(21) International Application Number:
PCT/EP2005/052685

(22) International Filing Date: 9 June 2005 (09.06.2005)

(25) Filing Language: English

(26) Publication Language: English

(30) Priority Data:
60/578,869 14 June 2004 (14.06.2004) US

(71) Applicants *(for all designated States except US)*: **UNIVERSITE DE LIEGE** [BE/BE]; Interface Entreprises-Université, Antheunis Nicole, Quai van Beneden 25, B-4020 Liege (BE). **BRIGHAM AND WOMEN'S HOSPITAL** [US/US]; 1249 Boylston Street, 2nd Floor, Boston, MA 02215 (US).

(72) Inventors; and

(75) Inventors/Applicants *(for US only)*: **VERLY, Jacques** [BE/BE]; Rue Belle-Jardinière 386/11, B-4031 Angleur (BE). **VIGNERON, Lara** [BE/BE]; Rue Charles Morren 11, B-4000 Liege (BE). **DUFLOT, Marc** [BE/BE]; Chienrue 19, B-4160 Anthisnes (BE). **WARFIELD, Simon** [US/US]; 173 Winchester Street, Brookline, MA 02446 (US).

(74) Common Representative: **UNIVERSITE DE LIEGE**; Interface Entreprises-Université, Antheunis Nicole, Quai van Beneden 25, B-4020 Liege (BE).

(81) Designated States *(unless otherwise indicated, for every kind of national protection available)*: AE, AG, AL, AM, AT, AU, AZ, BA, BB, BG, BR, BW, BY, BZ, CA, CH, CN, CO, CR, CU, CZ, DE, DK, DM, DZ, EC, EE, EG, ES, FI, GB, GD, GE, GH, GM, HR, HU, ID, IL, IN, IS, JP, KE, KG, KM, KP, KR, KZ, LC, LK, LR, LS, LT, LU, LV, MA, MD, MG, MK, MN, MW, MX, MZ, NA, NG, NI, NO, NZ, OM, PG, PH, PL, PT, RO, RU, SC, SD, SE, SG, SK, SL, SM, SY, TJ, TM, TN, TR, TT, TZ, UA, UG, US, UZ, VC, VN, YU, ZA, ZM, ZW.

(84) Designated States *(unless otherwise indicated, for every kind of regional protection available)*: ARIPO (BW, GH, GM, KE, LS, MW, MZ, NA, SD, SL, SZ, TZ, UG, ZM, ZW), Eurasian (AM, AZ, BY, KG, KZ, MD, RU, TJ, TM), European (AT, BE, BG, CH, CY, CZ, DE, DK, EE, ES, FI,

[Continued on next page]

(54) Title: METHOD FOR MODELLING THE DEFORMATION OF AN OBJECT AND APPARATUS THEREFOR;

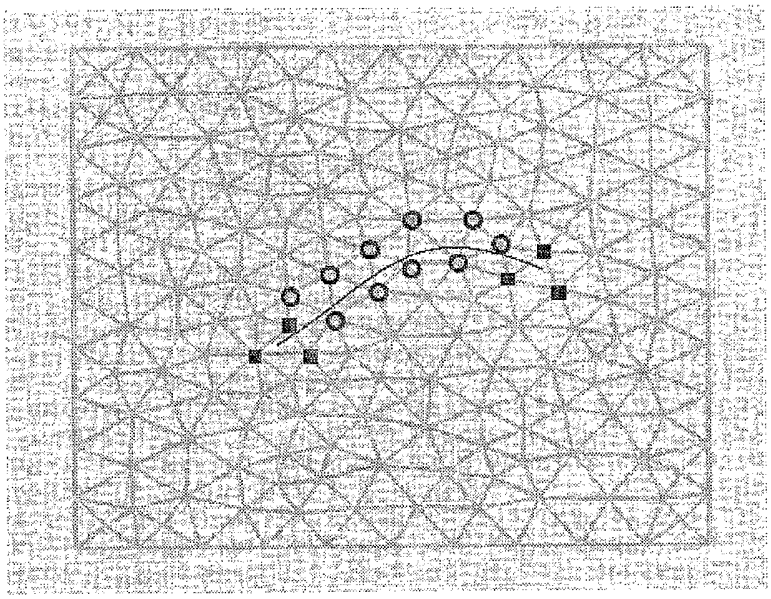

(57) Abstract: The invention provides a method for modelling the deformation of a deformable object subjected to a cut such as retraction or a resection, comprising the steps of creating a volume mesh of the deformable object in its initial form using standard finite element analysis meshing techniques, defining enrichment nodal shape function of the mesh elements that are intersected by the cut, and assembling a global stiffness matrix of the elements in the volume mesh using the stiffness matrix of the elements and the enrichment nodal shape functions. An electronic data processing apparatus operative according to the method is also provided.

WO 2005/122026 A2

FR, GB, GR, HU, IE, IS, IT, LT, LU, MC, NL, PL, PT, RO, SE, SI, SK, TR), OAPI (BF, BJ, CF, CG, CI, CM, GA, GN, GQ, GW, ML, MR, NE, SN, TD, TG).

Declarations under Rule 4.17:

— *as to applicant's entitlement to apply for and be granted a patent (Rule 4.17(ii)) for the following designations AE, AG, AL, AM, AT, AU, AZ, BA, BB, BG, BR, BW, BY, BZ, CA, CH, CN, CO, CR, CU, CZ, DE, DK, DM, DZ, EC, EE, EG, ES, FI, GB, GD, GE, GH, GM, HR, HU, ID, IL, IN, IS, JP, KE, KG, KM, KP, KR, KZ, LC, LK, LR, LS, LT, LU, LV, MA, MD, MG, MK, MN, MW, MX, MZ, NA, NG, NI, NO, NZ, OM, PG, PH, PL, PT, RO, RU, SC, SD, SE, SG, SK, SL, SM, SY, TJ, TM, TN, TR, TT, TZ, UA, UG, UZ, VC, VN, YU, ZA, ZM, ZW, ARIPO patent (BW, GH, GM, KE, LS, MW, MZ, NA, SD, SL, SZ, TZ, UG, ZM, ZW), Eurasian patent (AM, AZ, BY, KG, KZ, MD, RU, TJ, TM), European patent (AT, BE, BG, CH, CY, CZ, DE, DK, EE, ES, FI, FR, GB, GR, HU, IE, IS, IT, LT, LU, MC, NL, PL, PT, RO, SE, SI, SK, TR), OAPI patent (BF, BJ, CF, CG, CI, CM, GA, GN, GQ, GW, ML, MR, NE, SN, TD, TG)*

— *as to applicant's entitlement to apply for and be granted a patent (Rule 4.17(ii)) for the following designations AE, AG, AL, AM, AT, AU, AZ, BA, BB, BG, BR, BW, BY, BZ, CA, CH, CN, CO, CR, CU, CZ, DE, DK, DM, DZ, EC, EE, EG, ES, FI, GB, GD, GE, GH, GM, HR, HU, ID, IL, IN, IS, JP, KE, KG, KM, KP, KR, KZ, LC, LK, LR, LS, LT, LU, LV, MA, MD, MG, MK, MN, MW, MX, MZ, NA, NG, NI, NO, NZ, OM, PG, PH, PL, PT, RO, RU, SC, SD, SE, SG, SK, SL, SM, SY, TJ, TM, TN, TR, TT, TZ, UA, UG, UZ, VC, VN, YU, ZA, ZM, ZW, ARIPO patent (BW, GH, GM, KE, LS, MW, MZ, NA, SD, SL, SZ, TZ, UG, ZM, ZW), Eurasian patent (AM, AZ, BY, KG, KZ, MD, RU, TJ, TM), European patent (AT, BE, BG, CH, CY, CZ, DE, DK, EE, ES, FI, FR, GB, GR, HU, IE, IS, IT, LT, LU, MC, NL, PL, PT, RO, SE, SI, SK, TR), OAPI patent (BF, BJ, CF, CG, CI, CM, GA, GN, GQ, GW, ML, MR, NE, SN, TD, TG)*

Published:

— *without international search report and to be republished upon receipt of that report*

For two-letter codes and other abbreviations, refer to the "Guidance Notes on Codes and Abbreviations" appearing at the beginning of each regular issue of the PCT Gazette.

METHOD FOR MODELLING THE DEFORMATION OF AN OBJECT AND APPARATUS THEREFOR

The invention relates to a method for modelling the deformation of a deformable object that is subjected to cuts such as retractions, resections or similar operations, in any number and in any combination thereof. The method is general and may be adapted to a range of applications.

The invention also relates to the use of the method in a number of areas, such as, without limitation, solid mechanics, electromagnetics, hydraulics, surgical simulation, and surgical navigation, especially neurosurgery. The term 'modelling' is used in a generic way to mean predicting, computing, calculating, processing or any similar operation.

Background of the Invention

An object subjected to external forces will generally deform in response to these forces. In many applications, modelling the way the object deforms is of interest. The theories and mathematical tools for modelling the deformation of the object are found in the field of *solid mechanics*.

To model the deformation of a continuous object on an electronic data processing apparatus such as a computer, it is customary to have recourse to the *finite-element method (FEM)*. In fact, FEM is used, not only in solid mechanics, but also in other application areas such as electromagnetics and hydraulics. The basic idea of FEM, whatever its application area, is to divide a difficult problem into a series of simpler problems that are easier to solve. Then, the individual solutions can be assembled to solve the difficult problem.

Focusing on the example problem of modelling object deformation, the first step in applying FEM is to discretize the object, that is to decompose

the object into a series of discrete elementary volume elements. The result is a *volume mesh* of such elements. These elements can have arbitrary types of shapes. For the purpose of the present discussion and without any loss of generality, we assume that the elements are tetrahedral. (Other types of shapes are often used in various disciplines, such as mechanical engineering). The mesh is fully characterized by the position of all the mesh vertices (or nodes), by the lists of vertices making up each element in the mesh, and by the material making up each element.

The meshing of the object is the first step in the application of FEM. The second step is the FEM calculations, which can take several forms depending upon the application. The external forces acting upon the object can be arbitrary. The actual external forces can be thought of in terms of equivalent forces acting on all, or on some, of the nodes of the volume mesh. In simplified terms, FEM calculations allow the displacements of all the nodes of the volume mesh that result from the applied forces to be computed.

Once the displacements of the nodes have been obtained, the approximate displacement of any point in the object can be computed. The key to this last computation is in the nodal shape functions. Solving problems via FEM involves solving large systems of equations, but efficient techniques exist to do so. In some cases, instead of forces, the displacements imposed to the object may be given, such as on part of the object's surface. However, the principle remains essentially the same.

The more difficult case solved by the current invention is where discontinuities in the deformable object, such as cuts, including retractions and resections, and other related operations, are made in the real object and thus in the volume mesh that represents it.

Retraction is defined as the pulling on one or more sides of a cut and resection is defined as removing material from one or more sides of a cut. A major difference between a cut (and other related operations) and a crack, is that a crack occurs spontaneously and is typically uncontrolled, whereas a cut is the result of the interaction (generally intentional) of a media (such as a knife, a retractor, a resector, or a beam of radiation for example) with the deformable object. A cut is typically the result of a voluntary action and is typically controlled. Additionally, a crack generally propagates, while a discontinuity comprising a cut does not necessarily turn into a propagating discontinuity.

The notion of cut should not be construed as being limited to the physical action of cutting a physical object. Indeed, the notion of cut should be understood as any discontinuity that is voluntarily imposed on some entity. This entity can be, for example, a solid, a fluid, or an electromagnetic field.

FEM alone has proved unfeasible for solving deformation problems accurately and in real-time in such circumstances.

Additional background to the invention was initially developed in the field of fracture mechanics.

Fracture mechanics is primarly concerned with predicting when structures are likely to fail. Such failures can have catastrophic consequences such as the crash of a bridge, a building or an airplane. One particular manifestation of failure is the appearance of cracks.

Fracture mechanics is therefore primarily interested in determining the conditions, such as the loading levels, in which such cracks are likely to appear. Fracture mechanics is thus not primarily concerned with predicting the precise way cracks propagate and even less how the object

deforms on either side of the crack. Nevertheless, researchers have attempted to model the propagation of cracks using computation. Soon, they realized the limitations of standard FEM for dealing with cracks.

The reason why standard FEM is not suited for dealing with cracks is as follows. First, assume an initial volume mesh of an object (before any crack appears) has been produced. Then, assume that a crack appears and that the deformation of the object when it is subjected to external forces needs to be modelled. The simplest possible case, which is also totally unlikely in practice, is the one where the crack would exactly correspond to some facets of an ensemble of elements (e.g., some triangles of an ensemble of tetrahedra). Even in that case, FEM cannot be immediately applied. Indeed, one must first duplicate all the nodes along the crack, so that one side of the crack can move one way and the other side some other way.

The general case, which is almost certainly encountered in practice, is the one where the path of the crack is arbitrary. This implies that the crack most likely cuts across the elements (e.g., tetrahedra) in an arbitrary way. Before going further, it is important to be aware of the fact that a basic assumption of FEM is that the displacement field inside each element is necessarily continuous. Of course, this assumption is violated in the case of a crack since the forces applied to the object most likely imply a discontinuity in the displacement field across the crack. As a result, FEM cannot be used directly for crack problems.

Several solutions have been proposed to continue using FEM in the presence of cracks, such as remeshing the object, or adapting the mesh, but these solutions are all inefficient in terms of their computational requirements, data structure management, and use of computer memory.

Meshless methods were proposed as a way to resolve these issues relating to crack modelling.

The so called *extended finite-element method (XFEM)*, first published in 1999 by Moës et al, has been used specifically for studying and modelling cracks.

XFEM adds on a key technique to standard FEM. This technique is the enrichment of the displacement-field approximation of standard FEM. Using this approach, cracks can be dealt with without having to modify the original mesh, either partially or completely.

Being able to model, for example, the deformation of an organ during the course of surgery, either real or virtual, is of paramount importance. None of the prior techniques discussed above permit accurate, real-time modelling of these deformations.

There are other methods for dealing with deformation of objects such as the boundary-element method and mass-spring methods. However, they do not offer any advantage over FEM-based methods for dealing with cracks, cuts, and related operations.

Standard FEM and these other methods cannot model accurately and in real-time the deformation of a deformable object affected by cuts, and related operations, including, for example, retraction and resection. The invention solves this problem, as well as provides other benefits relating to, for example, the management of data structures and computer memory. The invention can be used in many new applications, including, for example, in surgery.

Summary of the Invention

According to one aspect of the invention, there is provided a method for modelling the deformation of a deformable object subjected to a cut such as involved in a retraction or a resection, comprising the steps of creating a volume mesh of the deformable object in its initial form using standard finite element analysis meshing techniques, defining enrichment nodal shape functions of the mesh elements that are intersected by the cut, and assembling a global stiffness matrix of the elements in the volume mesh using the stiffness matrix of the elements and the enrichment nodal shape functions.

Preferably each enrichment nodal shape function comprises a finite element nodal shape function that is multiplied by a discontinuous function.

Preferably the enrichment comprises adding to the enriched nodes new degrees of freedom that are associated with an enrichment nodal shape function, the number of degrees of freedom of an enriched node being greater than the number of degrees of freedom of a non-enriched node.

Preferably the approximation of the field of displacement does not interpolate nodal displacements for enriched nodes.

Preferably the enrichment nodal shape functions of the mesh elements that are intersected by the cut comprise a Heaviside function taking the form:

$$H(x)=\begin{cases}1 & for \quad (x-x^*).e_n>0\\ -1 & for \quad (x-x^*).e_n<0\end{cases} \qquad (10)$$

where x is a sample point of the deformable object, x* is the point on the cut that is the closest to x, and e_n is the outward normal to the cut at x*.

Preferably the method comprises a step of defining an enrichment nodal shape function of each mesh element that contains a tip of the cut.

Preferably each cut tip enrichment function comprises a function that incorporates the radial and angular behaviours of the asymptotic cut displacement field.

Preferably each enrichment nodal function of the mesh elements containing a cut tip takes the form:

$$\{F(r,\theta)\}_{L=1}^{4} = \{\sqrt{r}\sin(\frac{\theta}{2}), \sqrt{r}\cos(\frac{\theta}{2}), \sqrt{r}\sin(\frac{\theta}{2})\sin(\theta), \sqrt{r}\cos(\frac{\theta}{2})\sin(\theta)\}, \quad (11)$$

where r and θ are the local polar coordinates.

Even though the preferred use of the method is in 3D space, the method can be used in a space of arbitrary dimensionality, including 2D.

The above method is potentially useful in many application areas including, for example, solid mechanics (including in surgery), electromagnetics, hydraulics, surgical simulation, surgical image-guided navigation, and neurosurgery.

According to another aspect of the invention there is provided an electronic data processing apparatus controlled by a program to model the deformation of a deformable object subjected to a cut such as a retraction or a resection, using a method comprising the steps of creating a volume mesh of the deformable object in its initial form using standard finite element analysis meshing techniques, defining enrichment nodal shape functions of the mesh elements that are intersected by the cut, and assembling a global stiffness matrix of the elements in the volume mesh

using the stiffness matrix of the elements and the enrichment nodal shape functions.

Preferably the program of the electronic data processing apparatus is operative such that the computation of the deformation allows the rendering of the deformable object in an augmented-virtuality environment.

Preferably the electronic data processing apparatus comprises a visual display unit operative to display the deformable object as rendered by the program.

Preferably the computation of the deformation by the electronic data processing apparatus allows initial imagery of the deformable object to be updated in real-time.

According to another aspect of the invention there is provided a surgical guidance and simulation apparatus for modelling a retraction discontinuity and/or a resection discontinuity in an organ, the apparatus comprising an electronic data processor operative to process information relating to the geometry of the discontinuity and the displacement constraints along the organ surfaces and the discontinuity boundary, to determine the incision surface which allows the insertion of a retractor or a resector, the electronic data processor being further operative to generate a finite element analysis model comprising a mesh of the organ and associated shape functions of the nodes of the mesh, and, based upon the precise geometry of the discontinuity, to add enrichment shape functions to some of the existing nodes and then to solve the equations to provide an output indicative of the displacement at all points along the discontinuity as well as throughout the volume of the organ and its surface .

Preferably the finite element mesh is built without taking the discontinuity into account.

Preferably each enrichment nodal shape function comprises a finite element nodal shape function that is multiplied by a discontinuous function.

Preferably the enrichment comprises adding to the enriched nodes new degrees of freedom that are associated with an enrichment nodal shape function, the number of degrees of freedom of an enriched node being greater than the number of degrees of freedom of a non-enriched node.

Preferably the electronic data processor does not interpolate nodal displacements for enriched nodes.

Preferably the electronic data processor is operative to enrich nodes of the mesh elements that are intersected by the discontinuity using a Heaviside function taking the form:

$$H(x) = \begin{cases} 1 \ for \ (x - x^*).e_n > 0 \\ -1 \ for \ (x - x^*).e_n < 0 \end{cases} \quad (10)$$

where x is a sample point of the organ, x* is the point on the discontinuity that is the closest to x, and e_n is the outward normal to the discontinuity at x*.

Preferably the method comprises a step of defining an enrichment nodal shape function of each mesh element that contains a tip of the discontinuity.

Preferably each tip of the cut enrichment function comprises a function that incorporates the radial and angular behaviours of the asymptotic discontinuity displacement field.

Preferably each enrichment nodal function of the mesh elements containing a tip of the cut takes the form:

$$\{F(r,\theta)\}_{i=1}^{4} = \{\sqrt{r}\sin(\frac{\theta}{2}), \sqrt{r}\cos(\frac{\theta}{2}), \sqrt{r}\sin(\frac{\theta}{2})\sin(\theta), \sqrt{r}\cos(\frac{\theta}{2})\sin(\theta)\}, \quad (11)$$

where r and θ are the local polar coordinates.

Even though the preferred use of the method is in 3D space, the method can be used in a space of arbitrary dimensionality, including 2D.

The above method is potentially useful in many application areas including, for example, solid mechanics (including in surgery), electromagnetics, hydraulics, surgical simulation, surgical image-guided navigation, and neurosurgery.

According to a further aspect of the invention, there is provided a method for modelling the deformation of a deformable object subjected to a cut, the method comprising the steps of defining a mesh of the object using finite element analysis, defining the cut geometry by identifying the mesh elements that are fully intersected by the cut and the mesh elements that contain a cut tip, enriching the nodes of the mesh elements intersected by the cut with a Heaviside function, enriching the nodes of the mesh elements that contain a tip of the cut with a tip of the cut function, defining the number of degrees of freedom for each node, computing each elementary stiffness matrix, and using the node enrichment functions to subsequently assemble a global stiffness matrix of the deformable object.

Preferably where the method is used to model an object in 2D, the method defines the number of degrees of freedom as being two for a non-enriched node, four for a Heaviside-function-enriched node and ten for a crack-tip-functions-enriched node.

Preferably each enrichment nodal shape function comprises a finite element nodal shape function that is multiplied by a discontinuous function.

Preferably the method does not interpolate nodal displacements for enriched nodes.

Preferably the Heaviside function takes the form:

$$H(x)=\begin{cases}1 & for\ \ (x-x^*).e_n>0\\ -1 & for\ \ (x-x^*).e_n<0\end{cases} \qquad (10)$$

where x is a sample point of the deformable object, x* is the point on the cut that is the closest to x, and e_n is the outward normal to the cut at x*.

Preferably each cut tip enrichment function comprises a function that incorporates the radial and angular behaviours of the asymptotic cut displacement field.

Preferably each enrichment nodal function of the mesh elements containing a cut tip takes the form:

$$\{F_l(r,\theta)\}_{l=1}^{4}=\{\sqrt{r}\sin(\frac{\theta}{2}),\sqrt{r}\cos(\frac{\theta}{2}),\sqrt{r}\sin(\frac{\theta}{2})\sin(\theta),\sqrt{r}\cos(\frac{\theta}{2})\sin(\theta)\}, \qquad (11)$$

where r and θ are the local polar coordinates.

Even though the preferred use of the method is in 3D space, the method can be used in a space of arbitrary dimensionality, including 2D.

According to another aspect of the invention, there is provided an electronic data processing apparatus controlled by program means to model the deformation of a deformable object subjected to a cut by defining a mesh of the object using finite element analysis, defining the cut geometry by identifying the mesh elements that are fully intersected by the cut and the mesh elements that contain a cut tip, enriching the nodes of the mesh elements intersected by the cut with a Heaviside function, enriching the nodes of the mesh elements that contain a tip of the cut with a tip of the cut function, defining the number of degrees of freedom for each node, computing each elementary stiffness matrix, and using the node enrichment functions to subsequently assemble a global stiffness matrix of the deformable object.

Figure 1(a) is a schematic view of the coordinates of a Heaviside function corresponding to a crack discontinuity in a 2D case;

Figure 1(b) is a view corresponding to Figure 1 (a) of the local coordinates of the crack-tip enrichment functions;

Figure 2(a) shows the mesh and crack geometries before deformation;

Figure 2(b) shows the results of XFEM when displacements as given in equations (14) and (15) are applied along the crack;

Figure 3 shows a schematic view of a volume mesh of a deformable object having a discontinuity;

Figure 4(a) shows an image of an original 2D MRI image with cut (discontinuity) leading from the top surface to a tumour;

Figure 4(b) shows a binary image of the cortex extracted from (a);

Figure 4(c) shows a triangular mesh computed from (b); and

Figure 4(d) shows an image showing the result of deforming (a), masked with the region of (b), as specified by the retraction simulation described in the text.

Detailed Description of the Invention

Example I - Modelling of organ deformations associated with neurosurgery

Neurosurgeons plan surgery from patients' structural and functional images. During surgery, neuronavigation systems display the desired positions of surgical instruments in preoperative images. However, the brain deforms in the course of a surgery. These deformations occurs principally following the opening of the dura, the drainage of the cerebrospinal fluid (CSF), the retraction of tissues and the successive resections of, for example, a tumour.

The usefulness of prior neuronavigation systems is then limited because the current brain shape no longer corresponds to that of the preoperative images. Intraoperative image acquisition can partially circumvent this limitation by capturing the new shape of the brain, but such image acquisition is limited in signal-to-noise ratio and spatial resolution by the time constraints of the surgical procedure.

Additionally, not all imaging modalities (particularly functional ones) are available intraoperatively. Consequently, intraoperative monitoring and surgical navigation can be significantly improved by estimating the deformation of the brain and projecting preoperative imaging data into alignment with the subject brain.

Non-rigid registration techniques are numerous. One approach is to use biomechanical models to encapsulate the mechanical properties and behaviour of the brain. Intraoperative MRI images can be used to compute the displacements of the cortical and ventricular surfaces of the brain. The displacement field then drives the brain model in place of the forces acting on the brain. Deformations throughout the brain are calculated using the finite element method (FEM), e.g., with a linear elastic behaviour law. Other more complex behaviours can be considered, e.g., visco-elastic, poro-elastic.

Some past studies on brain deformation modelling have focused on the brain shift at an early stage of the procedure, before significant resection has taken place. The precision achieved in the prediction of displacements in this particular context are good, with for instance, landmark matching errors of 0.8 ± 0.4 mm at the surface of the brain and 1.1 ± 0.7 mm for the interior (mean ± standard deviation), which is comparable to the size of the voxels.

In comparison, modelling of retraction and resection is still in its infancy. There have been limited investigations of the forces involved in these two surgical tasks. There has also been an effort to create a so-called "smart retractor" capable of measuring forces intraoperatively; this device has already shown promising results. Intraoperative images will be very useful when used in conjunction with this device. Intraoperative MRI and captured brain deformation has been used in the presence of resection, but the model of resection simply consisted of clipping the deformed brain with the resection cavity.

Conventional FEM has serious limitations for modelling the tissue discontinuities associated with the resection of a tumour as discussed above. The displacement field that is the solution of the finite-element

(FE) calculation must be continuous inside each FE. Furthermore, the displacement at any node may take on only one value.

Consequently, the modelling of a discontinuity requires that discontinuity boundaries be aligned with boundaries of the elements and that nodes lying on these boundaries be duplicated. Extensive work has been performed in the domain of surgical simulation on the problem of cutting of a FE mesh. Most of the proposed solutions and algorithms are based on a subdivision method. All elements intersected by the cut are divided into sub-elements in order to create a boundary of finite elements aligned with the cut. The subdivision is subject to the constraint of a good aspect ratio for the new elements.

The main drawback of this method is the rapid growth of the numbers of nodes and elements in the mesh. In addition to the subdivision calculation, the larger mesh size increases the computation time, and it is challenging to maintain computationally efficient parallel data structures as the mesh evolves. Of course, it is important to keep in mind that real-time performance is absolutely essential for surgical navigation and simulation and some other applications.

Alternative methods have been evaluated to avoid these dramatic changes in the mesh. For example, the mesh may be adapted to the geometry of the cut: some nodes are selected, and they are then relocated to cling as best as possible to the cut geometry. However, an offset can remain between the boundary formed by these relocated nodes and the cut. Element degeneracies can also happen. Depending on the method used, the distortion of the mesh can produce elements with unacceptably large aspect ratios. One solution is a remeshing, but this will in turn lead to an increase in the computation time.

Review of Basic FEM Principles

The problem of finding the displacement field u(x) such that the weak form of the equations of linear elasticity is satisfied is equivalent to determining the displacement field which minimizes the total deformation energy E

$$E = \frac{1}{2}\int_{\Omega} \sigma\varepsilon \, d\Omega - \int_{\Omega} bu \, d\Omega - \int_{\Gamma_t} tu \, d\Gamma \qquad (1)$$

The quantities in (1) are as follows: $\varepsilon(x)$ and $\sigma(x)$ are the strain tensor and the stress tensor respectively, b(x) is the body force applied to the solid, while t(x) is the traction force applied to its surface. Ω represents the volume of the solid and Γt represents the surface of the solid on which traction is applied.

To solve the linear elastic problem, we need to discretize the equations. In particular, we need an approximation u^h for the displacement field u. The FEM approximation is defined by

$$u^h(x) = \sum_{i=1}^{N} \varphi_i(x) u_i \qquad (2)$$

where the u_i's are the discrete unknowns to be determined and the φ_i's are basis functions, called nodal shape functions. These functions must obey two conditions.

Firstly, φ_i has a compact support ω_i, which corresponds to the union of element subdomains connected to node i.

Secondly, we have

$$\varphi_i(x_j) = \begin{cases} 1 & if \quad i = j \\ 0 & if \quad i \neq j \end{cases} \quad on \quad \omega_i \qquad (3)$$

where the x_i's, i=1,...,N, are the coordinates of the nodes.

Equations (2) and (3) yield the following property

$$w^h(x_i) = \sum_{i=1}^{N} \varphi_i(x_i) u_i = u_i \qquad (4)$$

The FEM unknown u_i can be shown to be the displacement field value at the node x_i. The FEM displacement field interpolates nodal displacements.

Finally, the introduction of the FE approximation (2) in the minimization of equation (1) leads to the following system of linear equations

$$Ku = f \quad or \quad K_{ij} u_i = f_i \quad i,j = 1,...,n_i \qquad (5)$$

where

$$K_{ij} = \int_\Omega B_i^T H B_j \, d\Omega \quad with \quad \mathbf{B}_i = \begin{pmatrix} \frac{\partial \varphi_i}{\partial x} & 0 & 0 \\ 0 & \frac{\partial \varphi_i}{\partial y} & 0 \\ 0 & 0 & \frac{\partial \varphi_i}{\partial z} \\ \frac{\partial \varphi_i}{\partial y} & \frac{\partial \varphi_i}{\partial x} & 0 \\ 0 & \frac{\partial \varphi_i}{\partial z} & \frac{\partial \varphi_i}{\partial y} \\ \frac{\partial \varphi_i}{\partial z} & 0 & \frac{\partial \varphi_i}{\partial x} \end{pmatrix},$$

$$f_i = \int_\Omega \mathbf{b} \varphi_i \, d\Omega + \int_{\Gamma_t} \bar{t} \varphi_i \, d\Gamma$$

and H is Hooke's tensor. The final step is to solve equation (5) for the displacement u_i. Equation (2) can then be used to align preoperative and intraoperative images.

The following introduces the fundamental ideas of XFEM. The key of this method is to create a new displacement-field approximation by enriching the FE approximation (2), that is by multiplying some of the FE nodal shape functions by discontinuous functions. This enrichment can be made to take local form by only enriching those nodes whose support intersect a region of interest. We have

$$u^h(x) = \sum_{i \in I} \varphi_i(x) u_i + \sum_{i \in J} \varphi_i(x) \sum_{j=1}^{n^{Ei}} g_j(x) a_{ji} \quad (8)$$

The quantities in equation (8) are as follows: The φ_i's are the FE shape functions and the g_j's are the XFEM enrichment functions. We denote by I the set of all N nodes in the domain, and by J the subset of I corresponding to the n^E enriched nodes. u_i and a_{ji} are nodal DOFs and n^{Ei} denotes the number of enrichment functions for node i. The additional DOFs a_{ji} are associated with nodes that are enriched.

An important consequence of the XFEM function enrichment is that the approximation does not interpolate nodal displacements for enriched nodes x_i, i.e.,

$$u^h(x_i) = \sum_{i \in I} \varphi_i(x_i) u_i + \sum_{i \in J} \varphi_i(x_i) \sum_{j=1}^{n^{Ei}} g_j(x_i) a_{ji} = u_i + \sum_{j=1}^{n^{Ei}} g_j(x_i) a_{ji} \neq u_i \quad (9)$$

There is a choice of enrichment functions and enriched nodes that can be used.

We denote by Γ_d the crack surface. Any function that is discontinuous across Γ_d can be used to model an arbitrary discontinuity in u(x). The simplest choice is a piecewise-constant function that changes sign at the boundary Γ_d, the Heaviside function:

$$H(x)=\begin{cases}1 & for \quad (x-x^*).e_n>0\\ -1 & for \quad (x-x^*).e_n\le 0\end{cases} \qquad (10)$$

The coordinates of the Heaviside function corresponding to the crack discontinuity in a 2D case are shown in Figure 1(a). The local coordinates of the crack-tip enrichment functions are shown in Figure 1(b), where x is a sample point of the solid, x* is the point on the crack that is the closest to x, and e_n is the outward normal to the crack at x*.(Outward is defined in an obvious way based upon the relative positions of x and Γ_d.) The nodes that are enriched by this function are those for which the support intersects the crack.

However, this function is not sufficient to model accurately the tip of the crack when this tip terminates inside an element. Indeed, the node and so all of its support is enriched. Consequently, the crack would be modelled as though the crack-tip was extended till it intersects the element edge.

Consequently, nodes whose supports containing a crack-tip are not enriched with the Heaviside function, but with specific crack-tip enrichment functions that ensure that the crack terminates precisely at the location of the crack-tip. The crack-tip enrichment relies on functions that incorporate the radial and angular behaviour of the asymptotic crack-tip displacement field, which is two-dimensional by nature as shown in Figure 1(b):

$$\{F_l(r,\theta)\}_{l=1}^{4}=\{\sqrt{r}\sin(\frac{\theta}{2}),\sqrt{r}\cos(\frac{\theta}{2}),\sqrt{r}\sin(\frac{\theta}{2})\sin(\theta),\sqrt{r}\cos(\frac{\theta}{2})\sin(\theta)\}, \qquad (11)$$

where r and θ are the local polar-coordinates. (The first function is discontinuous on the crack faces.).

The XFEM approximation for a single pair of crack and crack-tip is thus:

$$u^h(x) = \sum_{i=1}^{N} \varphi_i(x) u_i + \sum_{j \in J} \varphi_j(x) H(x) a_j + \sum_{k \in K} \varphi_k(x) \left(\sum_{l=1}^{4} F_l(x) c_k^l \right), \quad (12)$$

The quantities in equation (12) are as follows. The u_i's are the nodal degrees of freedom (DOFs) associated with the continuous part of the FE solution, the a_j's are the nodal enriched DOFs associated with the Heaviside function, and the c_k^l's are the nodal enriched DOFs associated with the crack-tip functions. I is the set of all nodes in the mesh. J is the set of nodes whose shape function support is cut by the crack interior. K is the set of nodes whose shape function support is cut by the crack-tip x_c. With D denoting the crack geometry, we thus have the formal definitions:

$$K = \{k \in I : x_c \in \omega_k\} \qquad J = \{j \in I : \omega_j \cap D \neq \emptyset, j \notin K\}, \quad (13)$$

where ω_k denotes the compact support of the node k. The above equations can easily be generalized to several pairs of cracks and crack-tips.

To obtain the discrete XFEM equations equivalent to the FEM equations (5)-(7) we must substitute the approximation expression (12) in the total-energy expression (1) and minimize the resulting expression.

While FEM requires a remeshing and the duplication of nodes along the crack to take into account any discontinuity, XFEM requires identification of nodes belonging to the sets J and K and the computation of the stiffness matrice with enrichment functions. Because of the added nodal DOFs in XFEM, the stiffness matrix is larger than in FEM.

We have performed preliminary tests on simple 2D objects such as rectangles and ellipses containing a line-segment crack discontinuity. An exploratory program was written in Matlab. The Matlab PDE toolbox was used, but only to initialize a triangular mesh from a domain boundary.

The inputs to the program are the mesh definition and the crack geometry as shown in Fig. 2(a). The method begins by identifying the mesh elements that are fully intersected by the crack, and the mesh elements that contain a crack-tip. The number of DOFs for each node is then defined: two for a non-enriched node, four for a Heaviside-function-enriched node or ten for a near-tip-functions-enriched node. As with FEM, each elementary stiffness matrix is computed, taking into account the enrichment functions. The global stiffness matrix is subsequently assembled. The application of force or displacement constraints is performed in similar ways in both FEM and XFEM.

To illustrate the method, we have chosen to constrain the displacement along the (linear) crack. We have applied a displacement of (0.0266, 0.0103) and (-0.0266,-0.0103)[1] to each intersection, with the mesh, of the right and left crack lips, respectively. Each point is of the form (x,y), with the x and y axes being respectively horizontal and vertical in Fig. 2.

The intersection of the crack with the element containing the crack-tip was left free (i.e., no displacement was imposed) to avoid having excessive constraints near the tip. Indeed, we have noticed that element flipping can sometimes happen in this situation.

Figure 2a shows the mesh and crack geometries before deformation. Figure 2(b) shows the results of XFEM when displacements as given in equations (14) and (15) are applied along the crack.

The application of this displacement constraint is straightforward in XFEM. For the intersection (x_{int}) of an element defined by 3 nodes enriched with the Heaviside function, the relation between the nodal

DOFs[2] (We consider the intersection lying on the element boundary between node 1 with DOFs (u_{x1}, u_{y1}, a_{x1}, a_{y1}) and node 2 with DOFs (u_{x2}, u_{y2}, a_{x2}, a_{y2})) are:

$$\begin{cases} \varphi_1(x_{int})\,u_{x1} + \varphi_1(x_{int})\,a_{x1} + \varphi_2(x_{int})\,u_{x2} + \varphi_2(x_{int})\,a_{x2} = 0.0266 \\ \varphi_1(x_{int})\,u_{y1} + \varphi_1(x_{int})\,a_{y1} + \varphi_2(x_{int})\,u_{y2} + \varphi_2(x_{int})\,a_{y2} = 0.0103, \end{cases} \quad (14)$$

for the right lip where the Heaviside function (10) is equal to 1. Similarly, we have:

$$\begin{cases} \varphi_1(x_{int})\,u_{x1} - \varphi_1(x_{int})\,a_{x1} + \varphi_2(x_{int})\,u_{x2} - \varphi_2(x_{int})\,a_{x2} = -0.0266 \\ \varphi_1(x_{int})\,u_{y1} - \varphi_1(x_{int})\,a_{y1} + \varphi_2(x_{int})\,u_{y2} - \varphi_2(x_{int})\,a_{y2} = -0.0103, \end{cases} \quad (15)$$

for the left lip where the Heaviside function (10) is equal to -1. The result of these displacement constraints is an opening of the crack, which is illustrated in Fig. 2(b).

This example confirms that XFEM can elegantly and efficiently take into account (crack) discontinuities in the study of the mechanical properties of objects. In particular, no mesh adaptation or remeshing is required. In contrast with FEM, solution displacement fields can now contain discontinuities inside the finite elements.

The triangles that appear to have been added in Fig. 2(b) were added for display purposes only. They are needed to show the new boundary of the crack. However, none of these additional nodes or elements are involved in the XFEM calculation.

The above described method is particularly well adapted to deal with the general problem of cutting through a 2D or 3D finite-element mesh. This

is required to deal with discontinuities, e.g., cracks or cuts. The main feature of XFEM is that it can deal with discontinuities without having to perform computationally-expensive mesh adaptation or remeshing. Note that the technique applies to multiple discontinuities that have arbitrary locations and shapes.

The implications for surgical guidance and simulation are clear and significant. In surgery, the above described method could be very useful in the modelling of retraction and resection, each of these surgical procedures inducing discontinuities in tissues. The pieces of information needed are the discontinuity geometry and the displacement constraints along the organ surfaces and the discontinuity boundary. The incision surface allowing the insertion of the retractor can be determined by tracking. It can also be inferred from an intraoperative MRI image showing the retraction pathway. The displacements caused by the retractor can be calculated from distances between segmented brain boundaries along the retraction path and the calculated incision surface. The modelling of resection is more complicated given that the brain can swell during this surgical procedure and that this swelling is not visible in intraoperative images.

However, the difficult task of removing finite elements according to the boundary of resected areas can be done accurately with XFEM. Indeed, all elements falling entirely in the resected area can be removed. With the remaining elements, we can precisely specify the boundary of the resected cavity by adding discontinuous functions to nodes located along this boundary, which allows us to cancel the presence of the elements on the resected side of the boundary.

The invention proposes a new method for cutting meshes in arbitrary ways without mesh adaptation or remeshing, thereby avoiding the above

drawbacks. This method allows the object to be modeled by finite elements without explicitly meshing the cut surfaces. Discontinuities can then be arbitrarily located with respect to the underlying FE mesh.

In addition, no remeshing is required when the discontinuity changes shape. Other appealing features of the method are that the FEM framework and its advantages (sparsity and symmetry) are retained and that a single-field (displacement) variational principle is used.

Example II: Simulation of Surgical Retraction and Resection

Image-guided surgical navigation systems allow the surgeon to follow his planning more precisely by displaying the positions of surgical instruments in preoperative images. However, as surgery progresses, these images become inaccurate due to the deformations of organs. Even though intraoperative images can be acquired, they have limited signal-to-noise ratio and spatial resolution.

Additionally, not all imaging modalities (particularly functional ones) are available intraoperatively. Therefore, it is critical to continue using all preoperative images and to update them as organs deform.

Several non-rigid registration techniques could be potentially used for updating preoperative images. One approach is to model mechanical organ behaviour based on the finite element method (FEM). The idea is to capture the displacement of the surface(s) defining the shape of the organ and to compute the resulting deformation of a tetrahedron volume mesh of this organ by linear elastic finite element (FE) calculations.

To date, most of the studies of organ deformation based on biomechanical models have focused on the early stages of surgery, i.e., before any significant deformation has taken place and, especially, before any cut has

been performed. The precision achieved for deformation prediction is about 1 voxel. However, the situation becomes more complex when the surgeon performs cuts, retractions, or resections. Retraction and resection necessarily involve a cut. Therefore the question of modelling cuts and their effects is fundamental. The main difficulty associated with a cut is the discontinuity of matter displacement it involves. It is a significant obstacle that FEM does not provide for such discontinuities, so that other approaches must be sought.

This invention proposes a new approach to the problem of modelling the deformations of body organs that are being subjected to surgical cuts, retractions and resections. The key to our approach is the use of the extended finite element method (XFEM). This powerful method was introduced in 1999 by Moës et al in the field of "fracture mechanics". This field deals with the appearance of cracks, which should be viewed as material discontinuities, their geometry and their progression in mechanical structures such as airplanes wings. One particular advantage of XFEM is that it minimizes computational and memory requirements. Therefore, it may hold the key to real-time modelling of deformation in surgical simulation and navigation.

As discussed above, there are limitations in modelling cracks with FEM. Consider a solid, such as an organ, modelled by a volume mesh of elements, typically tetrahedra. The FEM approximation of the displacement u(x) of any point x in this solid is defined by:

$$u^h(x) = \sum_{i=1}^{N} \varphi_i(x) u_i, \qquad (1)$$

where i is the node index, N is the number of nodes in the mesh, u_i the displacement of node i, and φ_i the nodal shape function with compact support defined by the space occupied by all elements connected to node i. This space is called the nodal support of node i. The u_i 's are also referred as the nodal degrees of freedom (DOFs): these are the discrete unknowns solved for in the FEM computation.

The nodal shape functions φ_i (x) of FEM are defined to be continuous on each element. Therefore, there is no built-in way in FEM for handling a crack going through an element. The only solution is remeshing, which involves the addition of nodes and elements, or topology adaptation but these operations are computationally expensive. This makes FEM unsuitable for efficient crack modelling.

Previously, there have been three main methods for avoiding the drawbacks of FEM remeshing. The boundary element method (BEM) dates back to the 1960's and reached its peak of popularity in the 1980's. Originally, it was not designed or used for modelling cracks. The main feature of BEM is that it is based on the discretization of only the object surface. Since the volume is not meshed, the size of the corresponding set of equations is greatly reduced. However, these equations are non-symmetric and fully populated, which is in contrast to FEM.

BEM takes advantage of the fact that surface meshing is generally easier than volume meshing. When a crack appears and grows, new boundary elements must only be added along the crack. So BEM can avoid much of the remeshing required by FEM.

Meshless methods appeared in the 1970's but it is only since the 1990's that they have become the object of significant attention. Their goal is to address large deformation and crack problems. In FEM, the object of interest is represented by a mesh. The nodes interact because they are

connected together via the elements. In meshless methods, the object is represented by a set of non-connected nodes that interact because their shape functions overlap.

Several techniques exist to model a crack. They consist in cancelling the interaction between some nodes by limiting the influence domain of their shape functions. While the remeshing task is avoided, the computation of the shape functions and the quadrature associated with the weak form can lead to greater computational requirements than for FEM. Nevertheless, meshless methods are useful when a problem benefits from being solved with a displacement approximation that does not rely on mesh topology.

A biomechanical model of the heart subjected to large deformation due to cardiac motion has been recently studied with a meshless method.

First, an FEM model, i.e., a mesh and associated nodal shape functions, is built without taking the crack into account. Then, based upon the precise geometry of the crack, simple, auxiliary shape functions are added to some of the existing nodes. The solution of the equations can thus naturally provide a discontinuity in displacement at all points along the crack. The main appeal of XFEM stems from the fact that, without any remeshing, it can model the deformations due to cracks of arbitrary shapes and also the way they propagate through matter. The equations remain also sparse and symmetric. Since XFEM can be viewed as an extension of FEM, it is relatively simple to add XFEM capabilities to existing FEM frameworks.

XFEM works by allowing the solution of its equations to be discontinuous within mesh elements. An arbitrarily shaped crack can then be modelled without any remeshing. To provide a discontinuous solution, the displacement approximation $u^h(x)$ of equation (1) should be expressed, not only in terms of continuous FE shape functions $\varphi_i(x)$, but also in terms of some discontinuous functions. The key idea of XFEM is to enrich the

nodes whose support is fully or partially intersected by the crack. Enrichment is performed by adding DOFs to which one associates discontinuous shape functions.

Let us denote by Γ_d the surface of the crack. To model a discontinuity across Γ_d, a natural candidate is the Heaviside function, a piecewise-constant function that changes sign at the boundary Γ_d, i.e.,

$$H(x) = \begin{cases} 1 & for \quad (x - x^*).e_n > 0 \\ -1 & for \quad (x - x^*).e_n < 0 \end{cases} \qquad (2)$$

where x is a sample point of the solid, x* is the point on the crack that is the closest to x, and e_n is the unit outward normal to the crack at x*. This function is used when the nodal support is fully intersected by the crack. However, it is not suitable to model accurately the tip of the crack when this tip terminates inside an element. Indeed, if a node is enriched, the displacement approximation of every point x falling in its (nodal) support depends upon the Heaviside function. Thus, the crack would be modelled as though the "crack-tip" was extended till it intersects the boundary of the support.

Consequently, nodes that have a crack-tip within their support are enriched with specific crack-tip enrichment functions that incorporate the radial and angular behaviour of the two-dimensional asymptotic crack-tip displacement field. For an isotropic elastic material, the crack-tip functions

are:

$$\{F_l(r,\theta)\}_{l=1}^{4} = \{\sqrt{r}sin(\frac{\theta}{2}), \sqrt{r}cos(\frac{\theta}{2}), \sqrt{r}sin(\frac{\theta}{2})sin(\theta), \sqrt{r}cos(\frac{\theta}{2})sin(\theta)\}, \qquad (3)$$

where r and θ are the local polar coordinates (The first function is discontinuous at the surface of the crack.) These crack-tip functions ensure that the crack terminates precisely at the location of the crack-tip and that the model possesses a correct near-tip behaviour. The XFEM approximation for a single pair of crack and crack-tip is thus:

$$u^h(x) = \sum_{i \in I} \varphi_i(x) u_i + \sum_{j \in J} \varphi_j(x) H(x) a_j + \sum_{k \in K} \varphi_k(x) \left(\sum_{l=1}^{4} F_l(x) c_k^l \right), \quad (4)$$

where the u_i's are the nodal degrees of freedom (DOFs) associated with the continuous part of the FE solution, the a_j's are the nodal enriched DOFs associated with the Heaviside function, and the c_k^l's are the nodal enriched DOFs associated with the crack-tip functions. I is the set of all nodes in the mesh, J is the set of nodes whose shape function support is cut by the crack interior, and K is the set of nodes whose shape function support is cut by the crack-tip (Fig. 1).

The above equations can easily be generalized to several pairs of cracks and crack-tips.

Referring to Figure 3, the mesh and crack geometries are respectively shown in gray and black. The nodes enriched with Heaviside function are represented by a circle (set J) while nodes enriched with crack-tip functions are represented by a square (set K).

To evaluate the capabilities and the potential of our method for surgical simulation and navigation, we have performed preliminary tests on 2D objects containing a line-segment crack. The program was written in Matlab.

The inputs to the program are the mesh definition and the crack geometry. One begins by identifying the mesh elements that are fully intersected by the crack and the mesh elements that contain a crack-tip. One then defines the number of DOFs for each node: two for a non-enriched node, four for a Heaviside-function-enriched node or ten for a crack-tip-functions-enriched node. As with FEM, each elementary stiffness matrix is computed, taking into account the enrichment functions and the global stiffness matrix is subsequently assembled. The application of force or displacement constraints is performed in similar ways in both FEM and XFEM.

We conducted a series of experiments. First, we used simple geometric shapes. The triangular mesh was created using the Matlab PDE toolbox. Then, we used more realistic inputs.

We started from a segmented 3D image of the cortex and selected one of its horizontal slice as shown in Figure 4(a). The segmentation was performed and is shown in Figure. 2(b). The mesh was computed using the Distmesh2D tool as shown in Figure 4(c). The linear crack is shown in all images of Figure 4. It starts at the brain surface and finishes close to the tumour, defining an incision segment (surface in 3D).

To simulate the effect of a retractor (2D) that spreads out tissue from the incision segment, we proceed as follows. First, we compute the points of intersection of the crack with the mesh.

Then, we impose an arbitrary displacement of (-3.5,-1) and $(+3.5,+1)^3$ to each intersection, with the mesh, of the left and right crack lips, respectively. The intersection of the crack with the element containing the crack-tip was left free (i.e., no displacement was imposed) to avoid having

too large constraints near the tip. Indeed, we have noticed that element flipping generating element overlapping can sometimes happen in this situation.

The application of this displacement constraint in XFEM is straightforward. For the intersection (x_{int}) of the crack with an element defined by 3 nodes enriched with the Heaviside function, the relationship from equation (4) between the nodal DOFs[4] are:

$$\begin{cases} \varphi_1(x_{int})\,u_{x1} + \varphi_1(x_{int})\,a_{x1} + \varphi_2(x_{int})\,u_{x2} + \varphi_2(x_{int})\,a_{x2} = -3.5 \\ \varphi_1(x_{int})\,u_{y1} + \varphi_1(x_{int})\,a_{y1} + \varphi_2(x_{int})\,u_{y2} + \varphi_2(x_{int})\,a_{y2} = -1, \end{cases} \quad (5)$$

for the left lip, where the Heaviside function (2) is equal to +1.

Similarly, we have:

$$\begin{cases} \varphi_1(x_{int})\,u_{x1} - \varphi_1(x_{int})\,a_{x1} + \varphi_2(x_{int})\,u_{x2} - \varphi_2(x_{int})\,a_{x2} = 3.5 \\ \varphi_1(x_{int})\,u_{y1} - \varphi_1(x_{int})\,a_{y1} + \varphi_2(x_{int})\,u_{y2} - \varphi_2(x_{int})\,a_{y2} = 1, \end{cases} \quad (6)$$

Finally the discrete displacement solution provided by XFEM calculation was used to warp the brain image according to equation (4). The result of warping the image of Figure 4(a) masked with the region of Figure 4(b) is shown in Figure 4(d). Note that the image which was warped corresponds to the initial grayscale image Figure 4(a), but masked with the binary image Figure 4(b).

If one attempts to use standard FEM to cope with a material discontinuity, the computation time will increase significantly. Indeed one must modify the mesh in the vicinity of the discontinuity for the boundaries of the new elements to be aligned with the discontinuity, for the nodes on the discontinuity to be identified and duplicated, and for the matrices

representing the system of equations to be updated to take into account the new connectivity. In contrast, XFEM does not require remeshing.

While XFEM does require identification of the elements intersected by the crack and the use of the Heaviside function (2) requires a geometrical calculation, the primary expense is associated with the calculation of the elements of the stiffness matrix that are enriched. The dimension of elementary stiffness matrices can increase up to 30 x 30 for a triangular element with three nodes enriched by crack-tip functions as set out in equation (3), while a regular FEM representation always requires a 6 x 6 system. The stiffness matrix computation for an element including a node enriched with the crack-tip functions involves analytical computation of their derivatives and Gauss quadrature to numerically integrate over the element.

This invention comprises a new approach that totally avoids the need for remeshing. In contrast with FEM, the solution provided by XFEM can now contain a discontinuity of arbitrarily shape inside mesh elements. Since the underlying framework remains that of FEM, the equations remain sparse and symmetric, thereby maintaining the computational efficiency of FEM. Of course, the number of DOFs increases in the case of XFEM because of the node enrichment procedure. Since XFEM can be viewed as an extension of FEM, XFEM techniques can easily be incorporated into existing FEM-based codes and applications.

CLAIMS

1. A method for modelling the deformation of a deformable object subjected to a cut such as retraction or a resection, comprising the steps of creating a volume mesh of the deformable object in its initial form using standard finite element analysis meshing techniques, defining enrichment nodal shape functions of the mesh elements that are intersected by the cut, and assembling a global stiffness matrix of the elements in the volume mesh using the stiffness matrix of the elements and the enrichment nodal shape functions.

2. The method of claim 1 wherein each enrichment nodal shape function comprises a finite element nodal shape function that is multiplied by a discontinuous function.

3. The method of claim 2 wherein the enrichment comprises adding to the enriched nodes new degrees of freedom that are associated with an enrichment nodal shape function, the number of degrees of freedom of an enriched node being greater than the number of degrees of freedom of a non-enriched node.

4. The method of any one of claims 1 to 3 wherein the approximation of the field of displacement does not interpolate nodal displacements for enriched nodes.

5. The method of any one of the preceding claims wherein the enrichment nodal shape functions of the mesh elements that are intersected by the cut comprise a Heaviside function taking the form:

$$H(x) = \begin{cases} 1 & for \quad (x - x^*).e_n > 0 \\ -1 & for \quad (x - x^*).e_n < 0 \end{cases} \qquad (10)$$

where x is a sample point of the deformable object, x* is the point on the cut that is the closest to x, and e_n is the outward normal to the cut at x*.

6. The method of any one of the preceding claims wherein the method comprises a step of defining an enrichment nodal shape function of each mesh element that contains a tip of the cut.

7. The method of claim 6 wherein each cut tip enrichment function comprises a function that incorporates the radial and angular behaviours of the asymptotic cut displacement field.

8. The method of claim 7 wherein each enrichment nodal shape function of the mesh elements containing a cut tip takes the form:

$$\{F_l(r,\theta)\}_{l=1}^{4} = \{\sqrt{r}\sin(\tfrac{\theta}{2}), \sqrt{r}\cos(\tfrac{\theta}{2}), \sqrt{r}\sin(\tfrac{\theta}{2})\sin(\theta), \sqrt{r}\cos(\tfrac{\theta}{2})\sin(\theta)\}, \quad (11)$$

where r and θ are the local polar-coordinates.

9. The method of any one of the preceding claims wherein the modelling is in 3D space.

10. An electronic data processing apparatus controlled by a program to model the deformation of a deformable object subjected to a cut such as retraction or a resection, using a method comprising the steps of creating a volume mesh of the deformable object in its initial form using standard finite element analysis meshing techniques, defining enrichment nodal shape functions of the mesh elements that are intersected by the cut, and assembling a global stiffness matrix of the elements in the volume mesh using the stiffness matrix of the elements and the enrichment nodal shape functions.

11. The electronic data processing apparatus of claim 10 wherein the program is operative such that the computation of the deformation allows the rendering of the deformable object in an augmented-virtuality environment.

12. The electronic data processing apparatus of claim 11 comprising a visual display unit operative to display the deformable object as rendered by the program.

13. The electronic data processing apparatus of claim 12 wherein the computation of the deformation by the electronic data processing apparatus allows initial imagery of the deformable object to be updated in real-time.

14. A surgical guidance and/or simulation apparatus for modelling a retraction discontinuity and/or a resection discontinuity in an organ, the apparatus comprising an electronic data processor operative to process information relating to the geometry of the discontinuity and the displacement constraints along the organ surfaces and the discontinuity boundary, to determine the incision surface which allows the insertion of a retractor or a resector, the electronic data processor being further operative to generate a finite element analysis model comprising a mesh of the organ and associated shape functions of the nodes of the mesh, and, based upon the precise geometry of the discontinuity, to add enrichment shape functions to some of the existing nodes and then to solve the equations to provide an output indicative of the displacement at all points along the discontinuity.

15. The surgical guidance and simulation apparatus of claim 14 operative such that the finite element mesh is built without taking the discontinuity into account.

16. The surgical guidance and simulation apparatus of claim 14 and claim 15 wherein each enrichment nodal shape function comprises a finite element nodal shape function that is multiplied by a discontinuous function.

17. The surgical guidance and simulation apparatus of claim 16 wherein the enrichment comprises adding to the enriched nodes new degrees of freedom that are associated with enrichment nodal shape function, the number of degrees of freedom of an enriched node being greater than the number of degrees of freedom of a non-enriched node.

18. The surgical guidance and simulation apparatus of any one of claims 14 to 17 wherein the electronic data processor does not interpolate nodal displacements for enriched nodes.

19. The surgical guidance and simulation apparatus of any one of claims 14 to 18 wherein the electronic data processor is operative to enrich nodes of the mesh elements that are intersected by the discontinuity using a Heaviside function taking the form:

$$H(x)=\begin{cases}1 & for \quad (x-x^*).e_n>0\\ -1 & for \quad (x-x^*).e_n<0\end{cases} \qquad (10)$$

where x is a sample point of the organ, x* is the point on the discontinuity that is the closest to x, and e_n is the outward normal to the discontinuity at x*.

20. The surgical guidance and simulation apparatus of any one of claims 14 to 19 wherein the electronic data processor is operative to define an enrichment nodal shape function of each mesh element that contains a tip of the discontinuity.

21. The surgical guidance and simulation apparatus of claim 20 wherein each tip of the cut enrichment function comprises a function that incorporates the radial and angular behaviours of the asymptotic discontinuity displacement field.

22. The surgical guidance and simulation apparatus of claim 21 wherein each enrichment nodal function of the mesh elements containing a tip of the cut takes the form:

$$\{F_l(r,\theta)\}_{l=1}^{4} = \{\sqrt{r}\sin(\frac{\theta}{2}), \sqrt{r}\cos(\frac{\theta}{2}), \sqrt{r}\sin(\frac{\theta}{2})\sin(\theta), \sqrt{r}\cos(\frac{\theta}{2})\sin(\theta)\}, \quad (11)$$

where r and θ are the local polar-coordinates.

23. The surgical guidance and simulation apparatus of any one of claims 14 to 22 wherein the electronic data processor is operative to model the organ in 3D space.

24. A method for modelling the deformation of a deformable object subjected to a cut, the method comprising the steps of defining a mesh of the object using finite element analysis, defining the cut geometry by identifying the mesh elements that are fully intersected by the cut and the mesh elements that contain a cut tip, enriching the nodes of the mesh elements intersected by the cut with a Heaviside function, enriching the nodes of the mesh elements that contain a tip of the cut with a crack-tip function, defining the number of degrees of freedom for each node, computing each elementary stiffness matrix, and using the node enrichment functions to subsequently assemble a global stiffness matrix of the deformable object.

25. The method of claim 24, when used to model an object in 2D, comprising a step of defining the number of degrees of freedom as being

two for a non-enriched node, four for a Heaviside-function-enriched node and ten for a crack-tip-functions-enriched node.

26. The method of claim 24 to 25 wherein each enrichment nodal shape function comprises a finite element nodal shape function that is multiplied by a discontinuous function.

27. The method of any one of claims 24 to 26 wherein the method does not interpolate nodal displacements for enriched nodes.

28. The method of any one of claims 24 to 27 wherein the Heaviside function takes the form:

$$H(x)=\begin{cases}1 & for\ (x-x^*).e_n>0\\ -1 & for\ (x-x^*).e_n<0\end{cases} \quad (10)$$

where x is a sample point of the deformable object, x* is the point on the cut that is the closest to x, and e_n is the outward normal to the cut at x*.

29. The method of any one of claims 24 to 28 wherein each cut tip enrichment function comprises a function that incorporates the radial and angular behaviours of the asymptotic cut displacement field.

30. The method of claim 29 wherein each enrichment nodal function of the mesh elements containing a cut tip takes the form:

$$\{F_l(r,\theta)\}_{l=1}^4=\{\sqrt{r}\sin(\frac{\theta}{2}),\sqrt{r}\cos(\frac{\theta}{2}),\sqrt{r}\sin(\frac{\theta}{2})\sin(\theta),\sqrt{r}\cos(\frac{\theta}{2})\sin(\theta)\}, \quad (11)$$

where r and θ are the local polar-coordinates.

31. The method of any one of claims 24 to 30 wherein the object is modelled in 3D space.

32. An electronic data processing apparatus controlled by program means to model the deformation of a deformable object subjected to a cut by defining a mesh of the object using finite element analysis, defining the cut geometry by identifying the mesh elements that are fully intersected by the cut and the mesh elements that contain a cut tip, enriching the nodes of the mesh elements intersected by the cut with a Heaviside function, enriching the nodes of the mesh elements that contain a tip of the cut with a cut-tip function, defining the number of degrees of freedom for each node, computing each elementary stiffness matrix, and using the node enrichment functions to subsequently assemble a global stiffness matrix of the deformable object.

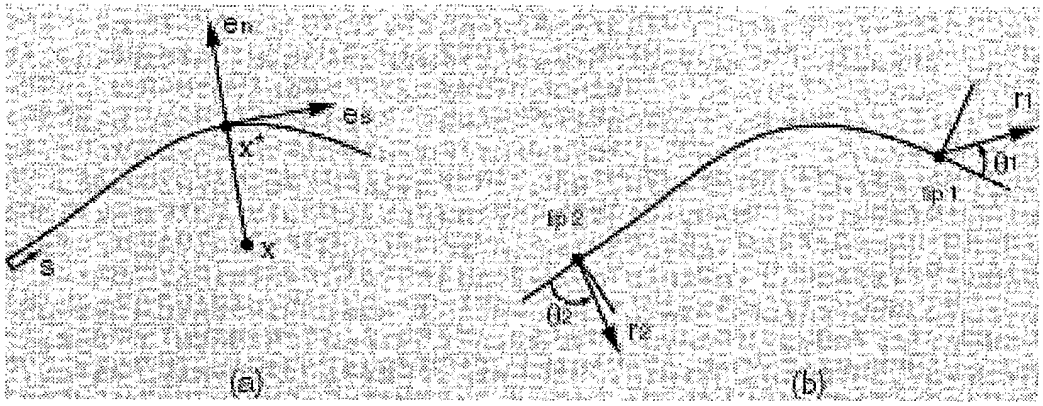

Fig 1

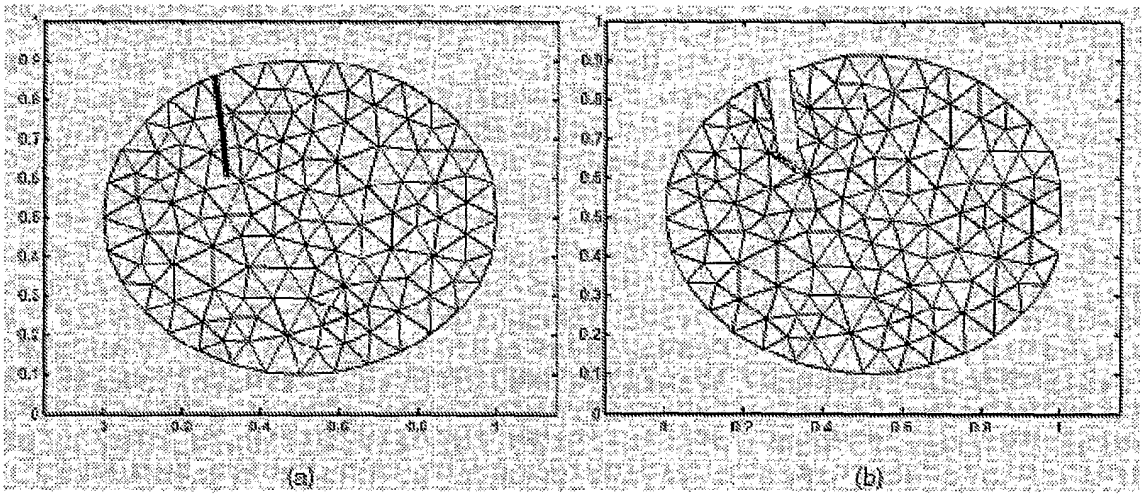

Fig 2

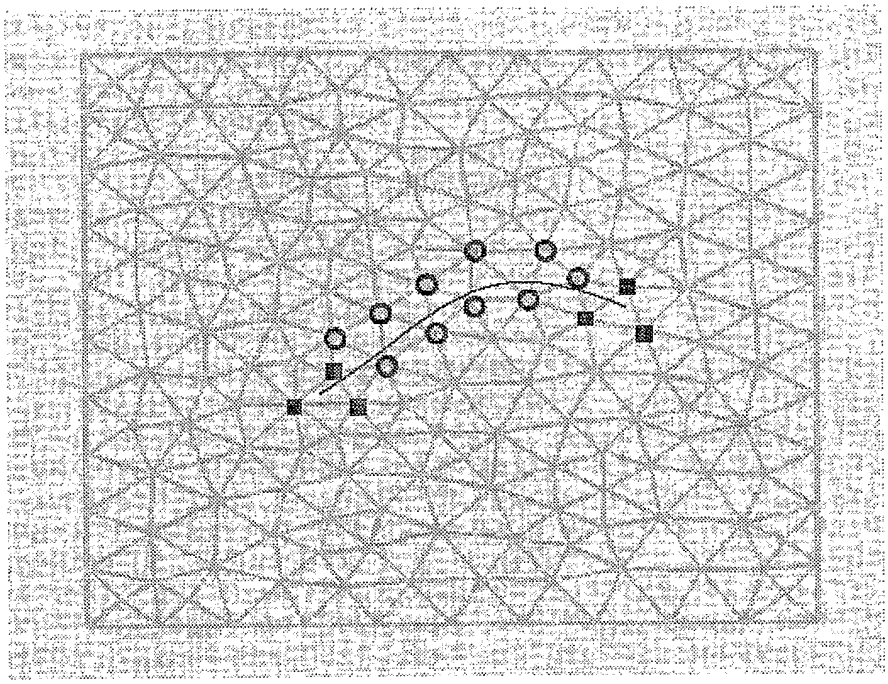

Fig 3

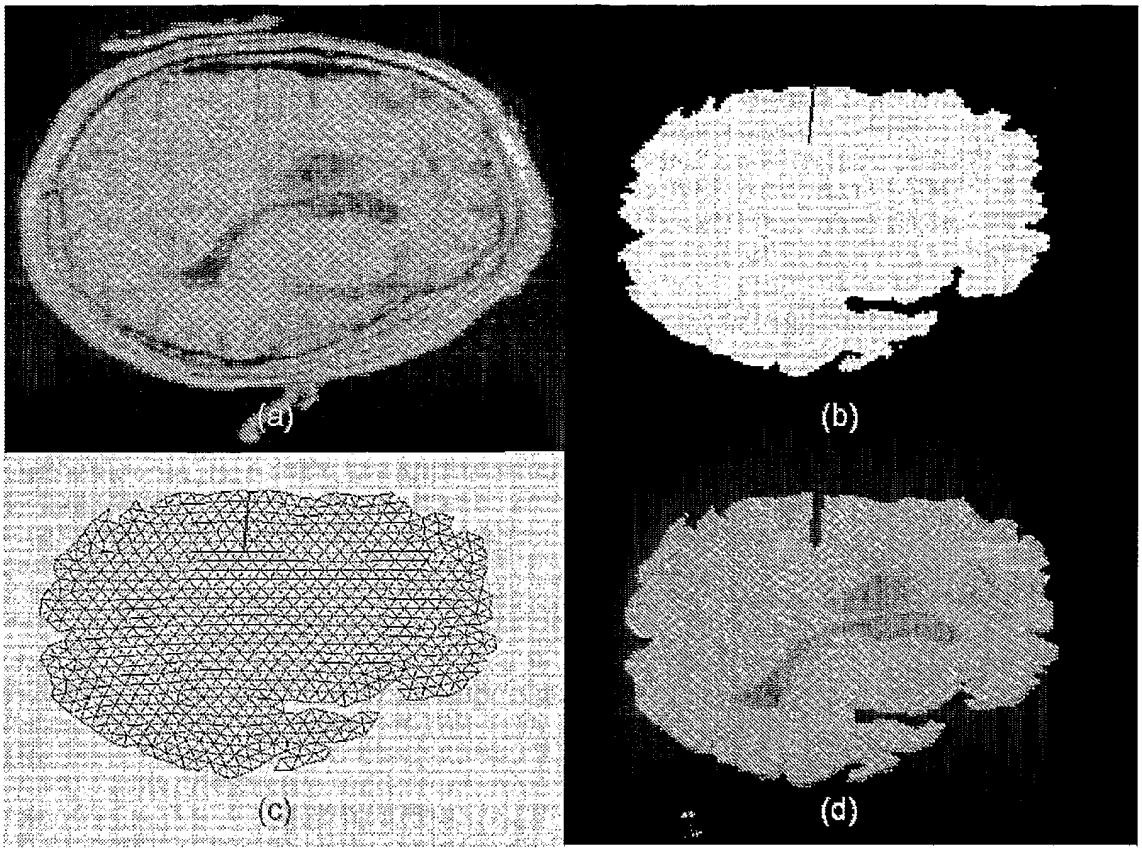

Fig 4